Systematic Investigation of Nitrile Based Ionic Liquids for CO2 Capture: A Combination of Molecular Simulation and ab Initio Calculation

ARTICLE *in* THE JOURNAL OF PHYSICAL CHEMISTRY C · JANUARY 2014

Impact Factor: 4.77 · DOI: 10.1021/jp411434g

2 AUTHORS:

Krishna Mohan Gupta
National University of Singapore
12 PUBLICATIONS **142** CITATIONS

SEE PROFILE

Jianwen Jiang
National University of Singapore
179 PUBLICATIONS **4,279** CITATIONS

SEE PROFILE

THE JOURNAL OF PHYSICAL CHEMISTRY C

Article

pubs.acs.org/JPCC

Systematic Investigation of Nitrile Based Ionic Liquids for CO_2 Capture: A Combination of Molecular Simulation and *ab Initio* Calculation

Krishna M. Gupta and Jianwen Jiang*

Department of Chemical and Biomolecular Engineering, National University of Singapore, 117576, Singapore

Supporting Information

ABSTRACT: Molecular simulation and *ab initio* calculation are performed to investigate CO_2 capture in four nitrile (−CN) based ionic liquids (ILs), namely 1-*n*-butyl-3-methylimidazolium thiocyanate [BMIM][SCN], 1-*n*-butyl-3-methylimidazolium dicyanamide [BMIM][$N(CN)_2$], 1-*n*-butyl-3-methylimidazolium tricyanomethane [BMIM][$C(CN)_3$], and 1-*n*-butyl-3-methylimidazolium tetracyanoborate [BMIM][$B(CN)_4$]. In neat ILs, the simulated densities match well with experimental data, and the cation−anion interaction becomes weaker with increasing number of −CN. In CO_2/IL systems, CO_2 molecules are preferentially located at the CO_2/IL interface, which is consistent with the observed minimum in the potential of mean force. The solubility and diffusivity of CO_2 in the four ILs increase as [BMIM][SCN] < [BMIM][$N(CN)_2$] < [BMIM][$C(CN)_3$] < [BMIM]-[$B(CN)_4$], thus increasing number of −CN is beneficial for CO_2 capture. CO_2 solubility is identified to be governed by the binding energy of cation−anion, rather than the binding energy of CO_2−anion. The computational study provides quantitative microscopic insight into the role of −CN in CO_2 sorption and diffusion, and it suggests that [BMIM][$B(CN)_4$] might be an interesting candidate for CO_2 capture.

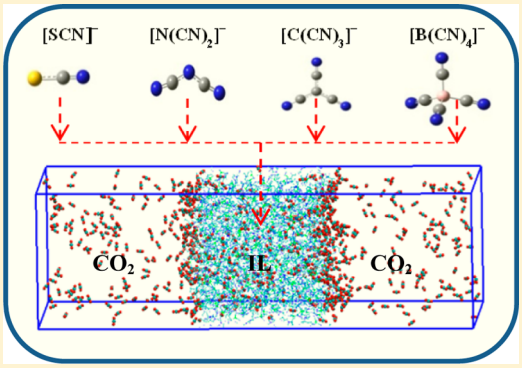

1. INTRODUCTION

Approximately 80% CO_2 emissions come from the combustion of fossil fuels.[1] The emissions are expected to increase because cheap and abundant fossil fuels will continue to be a substantial fraction of the energy portfolio. The International Panel on Climate Change (IPCC) predicted that the atmospheric CO_2 would increase up to 570 ppm in 2100, leading to a global temperature rise of 1.9 °C and a sea level increase of 38 cm.[2] Consequently, CO_2 capture from emissions has become a prime issue and there is an urgent need to reduce the carbon footprint for environmental protection and sustainable development.

Several techniques, such as amine scrubbing, cryogenic distillation, sorbent adsorption, and membrane separation, have been proposed for capture of CO_2. Among these, amine scrubbing is considered as an industrial benchmark for CO_2 capture.[3] However, there are several drawbacks in amine scrubbing, including degradation, corrosion, and intensive energy for regeneration. In the continuous quest of new surrogates for CO_2 capture, ionic liquids (ILs) have drawn significant attention.[4] ILs possess low melting points and usually exist in a liquid state at temperature below 100 °C. They are nonvolatile, nonflammable, thermally stable, and recognized as a unique class of solvents for many potential applications such as cellulose processing,[5,6] CO_2 capture,[7] electrochemistry,[8] biotechnology,[9] and lubricants.[10]

A large number of experimental and theoretical studies have been reported using ILs for CO_2 capture. For example, Blanchard et al. in 1999 first investigated the potential of ILs for CO_2 capture, and they reported that CO_2 solubility in 1-*n*-butyl-3-methylimidazolium hexafluorophosphate [BMIM][PF_6] could be achieved up to 0.6% at 8 MPa.[11] Brennecke and co-workers demonstrated that anions play a major role rather than cations in CO_2 sorption. Specifically, the hierarchy of CO_2 solubility in methyl-imidazolium based ILs follows $[NO_3]^-$ < $[DCA]^-$ < $[BF_4]^-$ ~ $[PF_6]^-$ < $[TfO]^-$ < $[Tf_2N]^-$ < [methide]$^-$.[12] By functionalizing ILs or tuning the basicity of ILs, Dai and co-workers synthesized task-specific ILs to enhance CO_2 solubility.[13,14] From simulation, Cadena et al. found that CO_2 is strongly associated with $[PF_6]^-$ rather than cation in imidazolium based ILs.[15] Babarao et al. reported that cation−anion interaction is more important than CO_2−anion interaction in determining CO_2 solubility.[16] The microscopic properties of IL and CO_2 at the IL/CO_2 interface were investigated by Maginn and co-workers.[17]

Among various types of ILs, nitrile (−CN) based ILs appear to be intriguing candidates for CO_2 capture. By combining experiment and a group-contribution approach, Carlisle et al. investigated CO_2 solubility and selectivity in ILs, and they observed that ILs functionalized by −CN exhibit higher CO_2/N_2 and CO_2/CH_4 selectivity relative to nonfunctionalized counterparts.[18] Gonzalez-Miquel et al. applied the COSMO-RS method to predict CO_2/N_2 selectivity in 224 ILs and illustrated that

Received: November 20, 2013
Revised: December 22, 2013
Published: January 17, 2014

   dx.doi.org/10.1021/jp411434g | J. Phys. Chem. C 2014, 118, 3110−3118

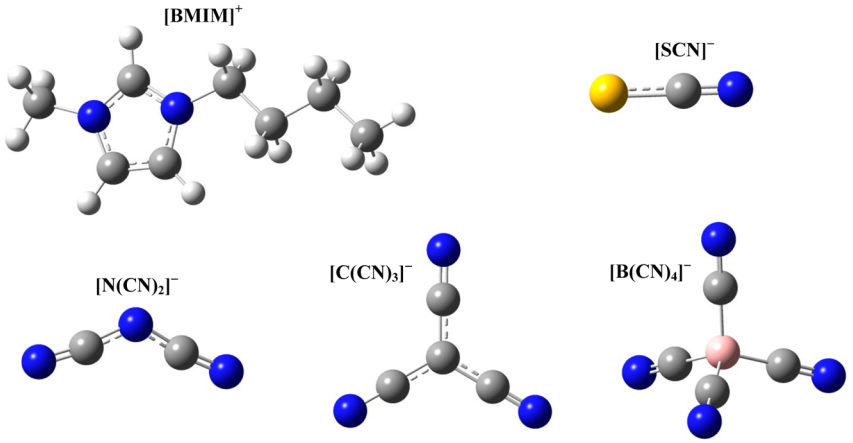

Figure 1. Structures of $[BMIM]^+$, $[SCN]^-$, $[N(CN)_2]^-$, $[C(CN)_3]^-$, and $[B(CN)_4]^-$. N, blue; C, cyan; O, red; S, yellow; B, pink; H, white.

$[SCN]^-$ based ILs can improve the selectivity.[19] Dai and coworkers explored the performance of a series of ILs containing −CN for CO_2/N_2 separation. They found $[B(CN)_4]^-$ based ILs possess high CO_2/N_2 selectivity and attempted to rationalize using the regular solution theory based on molar volume and viscosity of ILs.[20,21] By molecular simulation, we also revealed that $[SCN]^-$ anion is superior to a few other anions for CO_2 capture in MOF-supported IL membranes.[22] Despite these studies, it remains elusive how the −CN group in ILs would affect CO_2 capture, and there is no quantitative fundamental understanding.

A computational study is reported here to systematically investigate −CN based ILs for CO_2 capture. Specifically, four ILs are examined, namely 1-*n*-butyl-3-methylimidazolium thiocyanate [BMIM][SCN], 1-*n*-butyl-3-methylimidazolium dicyanamide $[BMIM][N(CN)_2]$, 1-*n*-butyl-3-methylimidazolium tricyanomethane $[BMIM][C(CN)_3]$, and 1-*n*-butyl-3-methylimidazolium tetracyanoborate $[BMIM][B(CN)_4]$. The four ILs possess the identical cation $[BMIM]^+$, but with different anions $[SCN]^-$, $[N(CN)_2]^-$, $[C(CN)_3]^-$, and $[B(CN)_4]^-$. We aim to provide microscopic insight into how the number of −CN groups in the anion systematically affects CO_2 sorption and diffusion. Following this introduction, the computational models and methods used are briefly described in section 2. The results are presented in section 3, including the equilibrium and dynamic properties of neat ILs, the sorption and diffusion of CO_2 in ILs, the potential of mean force for CO_2 moving into the IL phase, as well as the binding energies of CO_2−anion and cation−anion. Finally, the concluding remarks are summarized in section 4.

2. MODELS AND METHODS

2.1. Atomistic Models. Figure 1 illustrates the structures of [BMIM][SCN], $[BMIM][N(CN)_2]$, $[BMIM][C(CN)_3]$, and $[BMIM][B(CN)_4]$. The interactions of ILs are represented by bonded and nonbonded potentials. The bonded term includes stretching, bending, and torsional potentials

$$U_{\text{stretching}} = \sum \frac{1}{2} k_r (r_{ij} - r_{ij}^{\circ})^2 \quad (1)$$

$$U_{\text{bending}} = \sum \frac{1}{2} k_\theta (\theta_{ijk} - \theta_{ijk}^{\circ})^2 \quad (2)$$

$$U_{\text{torsional}} = \sum_{n=0}^{5} C_n [\cos(\phi_{ijkl} - 180)]^n \quad (3)$$

where k_r, k_θ, and C_n are the force constants; r_{ij}, θ_{ijk}, and ϕ_{ijkl} are bond lengths, angles, and dihedrals, respectively; and r_{ij}° and θ_{ijk}° are the equilibrium values. The nonbonded term consists of Lennard-Jones (LJ) and Coulombic potentials

$$U_{\text{nonbonded}} = \sum 4\varepsilon_{ij}\left[\left(\frac{\sigma_{ij}}{r_{ij}}\right)^{12} - \left(\frac{\sigma_{ij}}{r_{ij}}\right)^{6}\right] + \sum \frac{q_i q_j}{4\pi\varepsilon_0 r_{ij}} \quad (4)$$

where ε_{ij} and σ_{ij} are the well depth and collision diameter, r_{ij} is the distance between atoms i and j, q_i is the atomic charge of atom i, and $\varepsilon_0 = 8.8542 \times 10^{-12}$ C^2 N^{-1} m^{-2} is the permittivity of vacuum. For $[BMIM]^+$, $[SCN]^-$, $[N(CN)_2]^-$, and $[C(CN)_3]^-$, the bonded and LJ potential parameters were adopted from the AMBER force field.[23] For $[B(CN)_4]^-$, bonded potential parameters were provided by Borodin[24] without considering the polarization effect; and the LJ parameters for the B atom were taken from the DREIDING force field.[25] The atomic charges of ILs were estimated by density functional theory (DFT). The DFT calculations used the Becke exchange plus the Lee−Yang−Parr functional (B3LYP) implemented in the GAUSSIAN 09 package.[26] Each cation or anion was geometrically optimized at the 6-31G(d) basis set, and the electrostatic potentials were calculated at the 6-311+G(d,p) basis set. The atomic charges were then estimated by fitting to the electrostatic potentials with the Merz−Kollman scheme.[27] Supporting Information Figure S1 and Table S1 list the atomic types and charges of $[BMIM]^+$, $[SCN]^-$, $[N(CN)_2]^-$, $[C(CN)_3]^-$, and $[B(CN)_4]^-$.

2.2. Molecular Dynamics Simulations. Three sets of molecular dynamics (MD) simulations were conducted using GROMACS v.4.5.3.[28] The first set was to predict the equilibrium and dynamic properties of neat ILs. For each IL, the system was annealed from 500 to 350 K with a temperature interval of 50 K, and MD simulation was run for 2 ns at each temperature. Thereafter, the system was equilibrated at 298 K and 1 bar. To estimate the mobility of the cation/anion, however, the system was simulated at 400 K instead of 298 K. This is because the mobility at 298 K is small and cannot be reliably estimated; thus, the system was considered at high temperature, 400 K. The thermostat was governed by the velocity-rescaled Berendsen method with a relaxation time of 0.1 ps, whereas the barostat was maintained by the Berendsen method[29] with a relaxation time of 5 ps. The periodic boundary conditions were applied in all the dimensions. To calculate the Coulombic interactions, the particle-mesh Ewald method was adopted with a grid spacing of 0.12 nm and a fourth-order interpolation, while a spherical

dx.doi.org/10.1021/jp411434g | J. Phys. Chem. C 2014, 118, 3110−3118

cutoff of 1.4 nm was used to calculate LJ interactions. A time step of 1 fs was used to integrate the equations of motion by a leapfrog algorithm, and the trajectory was saved every 10 ps. The simulation duration was 20 ns, and the last 10 ns trajectory was used for analysis.

The second set of simulations was to examine CO_2 sorption in ILs. Figure 2 shows a typical simulation cell for the CO_2/IL system. In each system, CO_2 molecules were initially present in the gas phase and then gradually moved into the IL. The simulation was run in a NVT (canonical) ensemble at 298 K for 75 ns, and the last 10 ns trajectory was used for the ensemble average. Equilibrium was reached for CO_2 between gas phase and IL, and the number of CO_2 molecules in IL was counted as the solubility at the corresponding gas pressure. As discussed in section 3.2, the gas pressure was estimated to be 27 atm. The third set of simulations was performed to investigate CO_2 diffusion in ILs. Unlike the simulation cell in Figure 2, CO_2 and ILs were homogeneously mixed in this case. Table 2 lists the numbers of CO_2 molecules and ILs for four CO_2/IL systems. In each system, the number of CO_2 molecules was based on the solubility estimated from the second set of simulations. The simulation was conducted in a NPT ensemble for 20 ns at 298 K and 27 atm and then followed by another 20 ns run in a NVT ensemble. From the last 19 ns trajectory, CO_2 diffusivity was calculated.

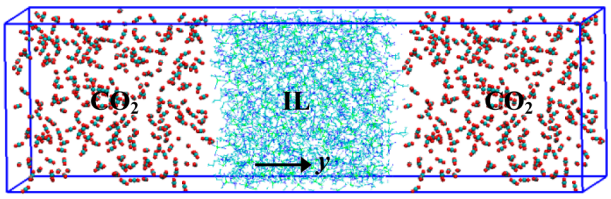

Figure 2. Typical simulation cell for the CO_2/IL system to examine CO_2 sorption.

system. The numbers of ILs and CO_2 molecules, as well as the cell dimensions, are listed in Table 1 for four CO_2/IL systems. In

Table 1. Numbers of IL and CO_2, and Cell Dimensions in CO_2/IL Systems To Examine CO_2 Sorption

system	no. of IL	no. of CO_2	cell dimensions
[BMIM][SCN]/CO_2	336	400	47 Å × 190 Å × 45 Å
[BMIM][N(CN)$_2$]/CO_2	336	450	50 Å × 190 Å × 44 Å
[BMIM][C(CN)$_3$]/CO_2	336	500	51 Å × 180 Å × 49 Å
[BMIM][B(CN)$_4$]/CO_2	336	600	53 Å × 180 Å × 52 Å

Table 2. Numbers of IL and CO_2 in CO_2/IL Systems To Examine CO_2 Diffusion

system	no. of IL	no. of CO_2
[BMIM][SCN]/CO_2	217	36
[BMIM][N(CN)$_2$]/CO_2	217	51
[BMIM][C(CN)$_3$]/CO_2	216	95
[BMIM][B(CN)$_4$]/CO_2	207	124

In addition, the potential of mean force (PMF) for CO_2 moving from gas phase to IL was evaluated. Specifically, umbrella sampling[30] was performed by considering 49 independent configurations with a successive increment of 1 Å along the y axis (see Figure 2). For each configuration, MD simulation was run for 5 ns. The test CO_2 molecule was harmonically restrained in a sampling window of spacing 1 Å, while other CO_2 molecules were allowed to move freely. To maintain a sufficient overlap between adjacent sampling windows, the harmonic biasing force constant was set to be 50 kJ mol^{-1} Å^{-2}. The PMF was evaluated by the weighted histogram analysis method (WHAM).[31]

2.3. *Ab Initio* Calculations. To elucidate CO_2 solubility and diffusivity in the four −CN based ILs, the binding energies of CO_2−anion and cation−anion were estimated from *ab initio* calculations using the GAUSSIAN 09 package.[26] However, the binding energies of CO_2−cation were not calculated because the cation plays a less important role in CO_2 solubility and the four ILs contain identical cation. The calculations used the second-order Møller−Plesset (MP2) method.[32] First, the structure of cation, anion, or CO_2 was optimized separately using the 6-31G basis set, as well as the structure of the complex (CO_2−anion or cation−anion). The optimization was followed by frequency calculation to ensure that the global minimum was achieved. Then, the single-point energy was calculated at a larger basis set of aug-cc-PVDZ. Finally, the binding energy was given by

$$\Delta E_{\text{binding}} = E_{\text{A-B}} - (E_{\text{A}} + E_{\text{B}}) \quad (5)$$

where A or B represents cation, anion, or CO_2; and A−B refers to complex. The basis set superposition errors (BSSE) were corrected by the common counterpoise method.[33]

3. RESULTS AND DISCUSSION

3.1. IL Systems. Table 3 lists the simulated densities of the four −CN based ILs at 298 K and 1 atm. Good agreement is observed with experimental data,[20,21,34] with less than 3% deviations. This suggests that the models used are, to a certain extent, reliable and accurate. The equilibrium structures of ILs are characterized by the radial distribution function $g(r)$

Table 3. Densities of ILs at 298 K and 1 atm

IL	density (kg/m^3) simulation	density (kg/m^3) experiment
[BMIM][SCN]	1100	1069[34]
[BMIM][N(CN)$_2$]	1071	1070[20]
[BMIM][C(CN)$_3$]	1062	1040[20]
[BMIM][B(CN)$_4$]	1034	1037[21]

$$g_{ij}(r) = \frac{N_{ij}(r, r + \Delta r)V}{4\pi r^2 \Delta r N_i N_j} \quad (6)$$

where r is the distance between atoms i and j, $N_{ij}(r, r + \Delta r)$ is the number of atoms j around i within a shell from r to $r + \Delta r$, V is the system volume, and N_i and N_j are the numbers of atoms i and j, respectively. Figure 3a shows the $g(r)$ of cation−anion in the four ILs, more specifically, the C_1 atom of cation around the N atom of anion. In each IL, two peaks at r = 3.3 and 5.3 Å are observed, particularly at 3.3 Å, indicating strong electrostatic attraction between cation and anion. Similar $g(r)$ was also observed in [BMIM][Ac], as shown in our previous study.[35] The structural arrangement of cation−anion is quantitatively the same in the four ILs; however, the primary difference is in peak height. With increasing the number of −CN, the height drops as $[SCN]^-$ > $[N(CN)_2]^-$ > $[C(CN)_3]^-$ > $[B(CN)_4]^-$. This indicates the hierarchy of cation−anion interaction strength is [BMIM][SCN] > [BMIM][N(CN)$_2$] > [BMIM][C(CN)$_3$] > [BMIM][B(CN)$_4$]. The reason is that with increasing the number of

dx.doi.org/10.1021/jp411434g | J. Phys. Chem. C 2014, 118, 3110−3118

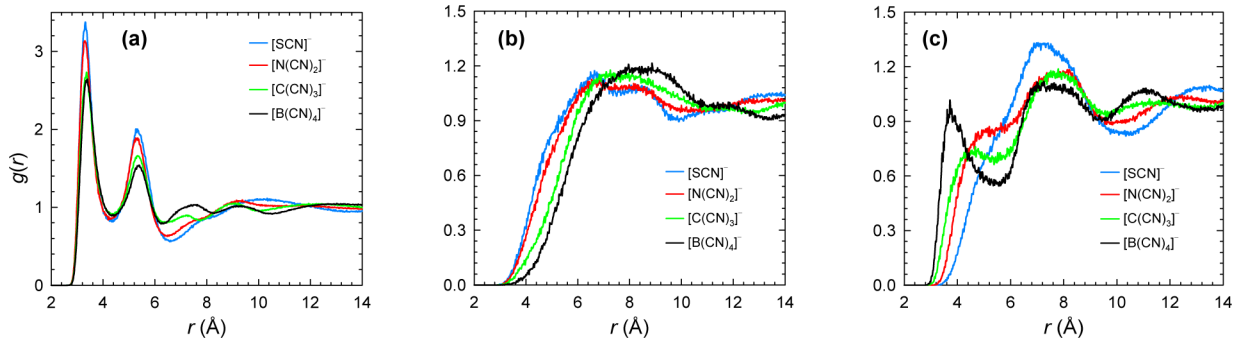

Figure 3. Radial distribution functions in ILs at 298 K: (a) cation−anion; (b) cation−cation; and (c) anion−anion.

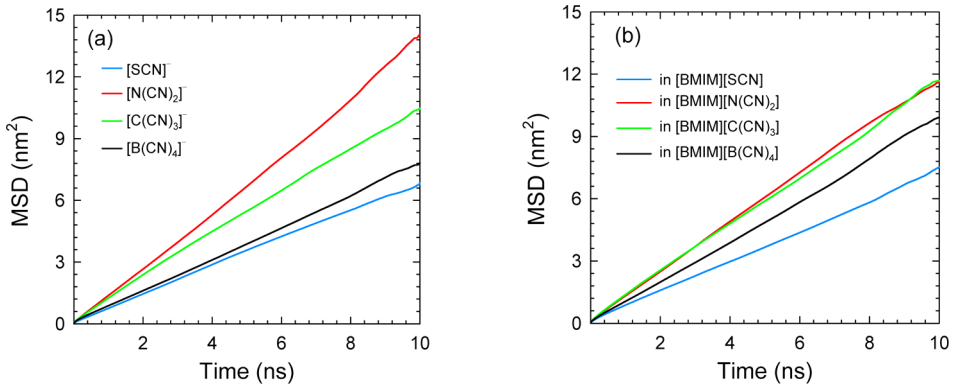

Figure 4. Mean-squared displacements of (a) anions and (b) cation in ILs at 400 K.

−CN in anion, the size of anion increases, leading to a decrease in cation−anion interaction. Quantitatively, the binding energies of cation−anion will be discussed in section 3.3. Figure 3b and c show the $g(r)$ of cation−cation and anion−anion. Due to unfavorable electrostatic repulsion, the $g(r)$ peaks are far less pronounced than in Figure 3a. For cation−cation, a broad shoulder is seen within 6.5−8.5 Å. For anion−anion, the $g(r)$ exhibits a moderately pronounced peak within 7−8 Å and decreases following $[SCN]^-$ > $[N(CN)_2]^-$ > $[C(CN)_3]^-$ > $[B(CN)_4]^-$, as seen in Figure 3a. The structural analysis implies that, by changing the number of −CN groups in anion, the cation−anion interaction is significantly altered, whereas both cation−cation and anion−anion interactions are moderately affected.

The dynamical properties of ILs are quantified by mean-squared displacement (MSD) and diffusivity. The MSD is defined as

$$\mathrm{MSD}(t) = \frac{1}{N}\sum_{i=1}^{N}\langle|\mathbf{r}_i(t) - \mathbf{r}_i(0)|^2\rangle \tag{7}$$

where N is the number of ions and $\mathbf{r}_i(t)$ is the position of the i^{th} ion at time t. To improve statistical accuracy, the multiple time-origin method was used to estimate the ensemble averaged MSDs. Figure 4a shows the MSDs of anions in ILs at 400 K. Intuitively, $[SCN]^-$ is the smallest in size as well as the lightest in weight; thus, its mobility would be the highest. Nevertheless, the MSD decreases in the order of $[N(CN)_2]^-$ > $[C(CN)_3]^-$ > $[B(CN)_4]^-$ > $[SCN]^-$; that is, $[SCN]^-$ has the smallest mobility. The reason for this counterintuitive phenomenon is that the mobility of anion depends on two factors: the size/weight of anion and its interaction with cation. As discussed above, $[SCN]^-$ has the strongest attraction with $[BMIM]^+$ among the four anions; it is thus largely bound with $[BMIM]^+$ and possesses the smallest mobility. Therefore, the mobility of $[SCN]^-$ is governed by $[SCN]^-$−$[BMIM]^+$ interaction rather than the size/weight of $[SCN]^-$. For $[N(CN)_2]^-$, $[C(CN)_3]^-$, and $[B(CN)_4]^-$, however, the size/weight of anion plays a dominant role. Figure 4b presents the MSDs of $[BMIM]^+$ in the four ILs. Despite identical cation, $[BMIM]^+$ exhibits different MSDs, but the trend is similar to those in Figure 4a. This implies that the mobility of $[BMIM]^+$ is substantially affected by the anion.

The MSDs were found to scale linearly with t, suggesting the occurrence of normal (or Einstein) diffusion. The diffusivities were thus estimated by

$$D = \frac{1}{6N}\frac{\mathrm{d}}{\mathrm{d}t}\lim_{t\to\infty}\sum_{i=1}^{N}\langle|\mathbf{r}_i(t) - \mathbf{r}_i(0)|^2\rangle \tag{8}$$

Table 4 lists the diffusivities of cation (D_+) and anions (D_-) in the four ILs. The magnitude of D_+ and D_- is 10^{-6} cm^2/s, similar to reported studies in the literature.[36−38] With increasing number of −CN, the trend of D_+ and D_- is similar to the MSD. The D_+ is higher than D_- except in $[BMIM][N(CN)_2]$. This observation is consistent with a previous simulation study, in which cations

Table 4. Diffusivities of Cation and Anion at 400 K

	D (10^{-6} cm^2/s)	
IL	D_+	D_-
[BMIM][SCN]	1.19	1.13
[BMIM][N(CN)$_2$]	1.98	2.29
[BMIM][C(CN)$_3$]	1.87	1.70
[BMIM][B(CN)$_4$]	1.65	1.29

dx.doi.org/10.1021/jp411434g | J. Phys. Chem. C 2014, 118, 3110−3118

were found to generally have higher diffusivities than anions in various ILs.[36]

3.2. CO_2/IL Systems. As described earlier, a simulation cell in Figure 2 was used to examine CO_2 sorption in ILs. CO_2 molecules gradually moved from gas phase (pure CO_2) to IL, and a typical final simulation snapshot is illustrated on the top of Figure 5. Also presented are the density profiles of CO_2 in four

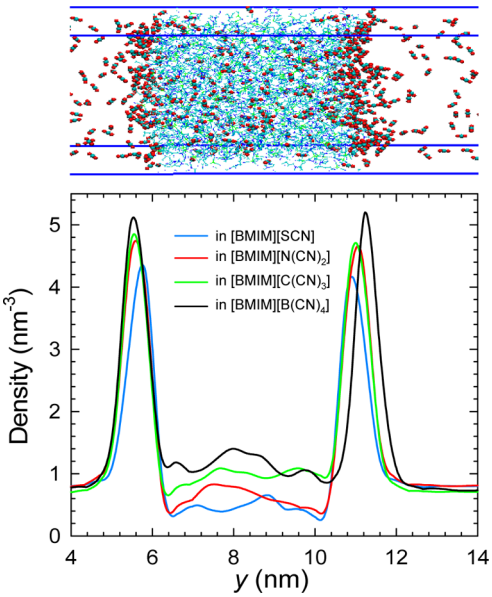

Figure 5. Density profiles of CO_2 in CO_2/IL systems along the *y*-axis. The top illustrates a typical simulation snapshot at equilibrium.

CO_2/IL systems. The density of CO_2 molecules in the gas phase is approximately identical in the four systems, equal to 0.8 nm^{-3}. From separate MD simulations, this density corresponds to a pressure of 27 bar in the gas phase. In each system, the maximum CO_2 density is located approximately at 55 and 110 Å, indicating CO_2 molecules are preferentially accumulated at the CO_2/IL interfacial region. Such behavior was observed in experiment by Roscioli and Nesbitt[39] and in simulation by Perez-Blanco and Maginn.[40] Roscioli and Nesbitt pointed out that the interfacial accumulation of CO_2 is attributed to strong CO_2–IL interaction, whereas CO_2 sorption in IL is governed by the free volume of IL.[39] Comparing the four systems, CO_2 densities in both the interfacial and IL region increase as [BMIM][SCN] < [BMIM]-[$N(CN)_2$] < [BMIM][$C(CN)_3$] < [BMIM][$B(CN)_4$]. Therefore, CO_2 solubility in the four –CN based ILs is enhanced by increasing the number of –CN in the anion. Although there are no exact experimental solubility data available for comparison, the trend of CO_2 solubility found here is consistent with experimental observation in [BMIM][$N(CN)_2$], [BMIM][C-($CN)_3$] and [BMIM][$B(CN)_4$].[20,21]

It is instructive to understand the locations of cation and anion at the CO_2/IL interface. Figure 6 shows the density profiles of cation and anions over a region y = 4–9 nm (see Figure 5) in CO_2/IL systems. The long butyl chain of $[BMIM]^+$ is represented by C_6, C_7, and C_8 atoms, whereas the short methyl group is denoted by C_4 atom (see Supporting Information Figure S1). In each CO_2/IL system, the profiles of C_6, C_7, and C_8 atoms exist at the outer edge of the interface; in contrast, the profile of C_4 atom resides at the inner edge. These features suggest that the hydrophobic butyl chain is located toward the gas phase, whereas the less hydrophobic methyl group favors the IL phase. The profile of the N atom in anion lies between the butyl and methyl

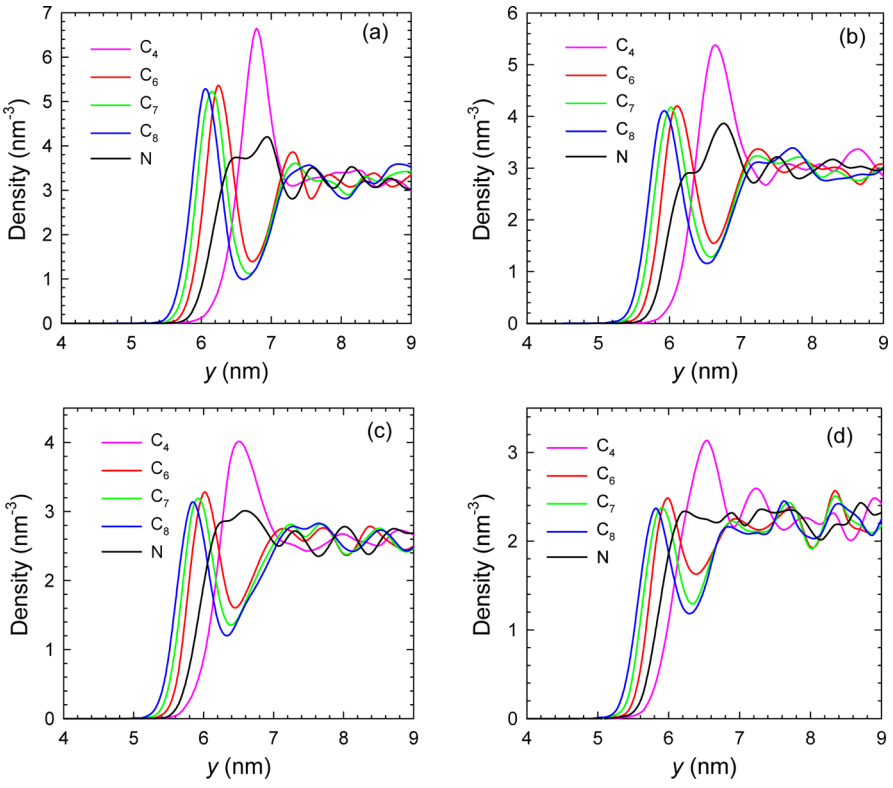

Figure 6. Density profiles of cation and anions in (a) CO_2/[BMIM][SCN], (b) CO_2/[BMIM][$N(CN)_2$], (c) CO_2/[BMIM][$C(CN)_3$], and (d) CO_2/[BMIM][$B(CN)_4$]. The cation is represented by C_4, C_6, C_7, and C_8 atoms, and the anion by N atom.

dx.doi.org/10.1021/jp411434g | J. Phys. Chem. C 2014, 118, 3110–3118

groups. A similar observation was also reported in a simulation study.[40] In addition, the peak height in the density profile depends on the type of IL, decreasing in the order of [BMIM][SCN] > [BMIM][N(CN)$_2$] > [BMIM][C(CN)$_3$] > [BMIM][B(CN)$_4$]. This implies that the clustering between cation and anion becomes weaker with increasing number of −CN, as elucidated in Figure 3a and as will be further discussed in section 3.3 on the basis of cation−anion binding energies.

The dynamics of CO_2 in ILs is assessed by diffusivity. As shown in Figure 7, the magnitude of D_{CO_2} in the four ILs is 10^{-6} cm^2/s, close to other ILs.[41] The D_{CO_2} increases in the order of [BMIM][SCN] < [BMIM][N(CN)$_2$] < [BMIM][C(CN)$_3$] < [BMIM][B(CN)$_4$], and this hierarchy will also be discussed in section 3.3. Combining with the CO_2 sorption illustrated in Figure 5, we can conclude that CO_2 has higher solubility and diffusivity in [BMIM][B(CN)$_4$] than in the other three −CN based ILs. Therefore, [BMIM][B(CN)$_4$] might be a promising candidate for CO_2 capture.

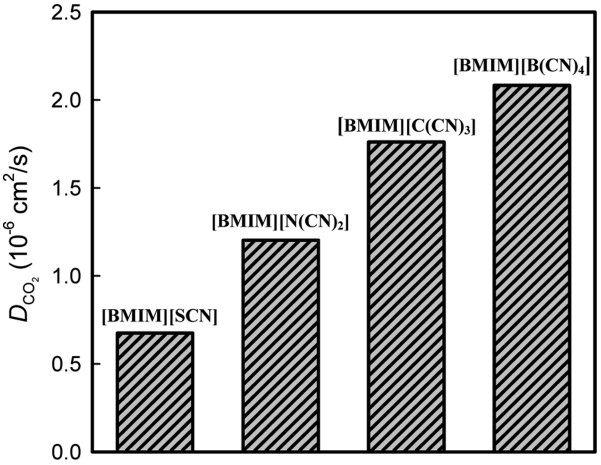

Figure 7. Diffusivities of CO_2 in ILs.

To quantitatively analyze how CO_2 moves from gas phase into IL, the potential of mean force (PMF) was calculated by

$$\mathrm{PMF}(y) = \int_{y_0}^{y} \langle F(y') \rangle \, \mathrm{d}y' \tag{9}$$

where $\langle F(y') \rangle$ is the ensemble averaged force acting on a molecule at position y'. The PMF(y) provides the work required for a molecule moving from a reference position y_0 to y along the y-axis. For the CO_2/[BMIM][B(CN)$_4$] system as shown in Figure 8, the PMF is nearly zero in the gas phase and decreases (more negative) upon moving toward the IL/CO_2 interface due to the favorable interactions with ions. At the interface, a minimum of −1.57 kcal mol^{-1} is observed. In the IL, the average PMF is approximately −0.45 kcal mol^{-1}. Consequently, the PMF at the interface is the strongest, which is in accord with the maximum density profile of CO_2 at the interface (see Figure 5). The minimum PMF of −1.57 kcal mol^{-1} is a driving force for CO_2 molecules to be preferentially located at the interface. A similar trend of PMF was observed for CO_2 crossing CO_2/[BMIM][BF_4] and CO_2/[BMIM][Tf_2N] interfaces.[42,43]

3.3. CO_2−Anion and Cation−Anion Binding Energies.

The above simulation results demonstrate that both solubility and diffusivity of CO_2 in the four −CN based IL increase as [BMIM][SCN] < [BMIM][N(CN)$_2$] < [BMIM][C(CN)$_3$] < [BMIM][B(CN)$_4$], i.e., with increasing number of −CN in the anion. To provide more fundamental insight, CO_2−anion binding energies were estimated by *ab initio* calculations. Nevertheless, CO_2−cation binding energies were not calculated because anion is more preferential than cation for CO_2 sorption, which can be seen in Supporting Information Figure S2 for the $g(r)$ of CO_2 around $[BMIM]^+$ and $[B(CN)_4]^-$ in the [BMIM][B(CN)$_4$]/CO_2 system. The $g(r)$ around $[B(CN)_4]^-$ exhibits a pronounced peak at r = 4.5 Å, whereas the peak around $[BMIM]^+$ is weak.

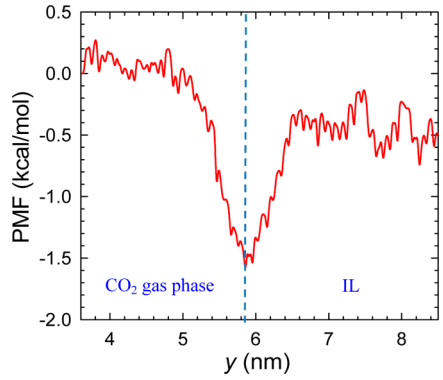

Figure 8. Potential of mean force for CO_2 moving from gas phase into [BMIM][B(CN)$_4$]. The dotted line represents the CO_2/IL interface.

Figure 9 shows the optimized configurations and binding energies of CO_2 with $[SCN]^-$, $[N(CN)_2]^-$, $[C(CN)_3]^-$, and $[B(CN)_4]^-$. The C atom in CO_2 is closer than the O atom to the N atom in −CN. The distance between the C and the N atoms increases in the order of $[SCN]^-$ < $[N(CN)_2]^-$ < $[C(CN)_3]^-$ < $[B(CN)_4]^-$; thus, $\Delta E_{CO_2-anion}$ decreases (i.e., becomes weaker) with increasing number of −CN. In principle, a weaker $\Delta E_{CO_2-anion}$ would lead to a lower solubility and a higher diffusivity for CO_2. This is true for CO_2 diffusivity in Figure 7, but not for CO_2 solubility in Figure 5. For example, $\Delta E_{CO_2-[B(CN)_4]^-}$ is the weakest among the four ILs; nevertheless, both the diffusivity and solubility of CO_2 in [BMIM][B(CN)$_4$] are the highest. Such a counterintuitive relation between CO_2 solubility and $\Delta E_{CO_2-anion}$ was also found in a few computational studies.[44,45] Apparently, CO_2 solubility is not governed by $\Delta E_{CO_2-anion}$. An *in situ* attenuated total reflectance IR (ATR-IR) study suggested that cation−anion binding energy $\Delta E_{cation-anion}$ plays a dominate role for CO_2 solubility in [BMIM][PF_6].[46] To understand high CO_2 solubility in a tetracyanoborate-containing IL, Babarao et al. showed that CO_2 possesses a higher solubility in an IL with a lower $\Delta E_{cation-anion}$.[16]

To further elucidate the tread of CO_2 solubility in the four −CN based ILs, Figure 10 shows the optimized configurations and binding energies of $[BMIM]^+$ with $[SCN]^-$, $[N(CN)_2]^-$, $[C(CN)_3]^-$, and $[B(CN)_4]^-$. The magnitude of $\Delta E_{cation-anion}$ is much higher than that of $\Delta E_{CO_2-anion}$ due to the favorable electrostatic interaction between cation and anion. With increasing number of −CN, $\Delta E_{cation-anion}$ decreases as $[BMIM]^+$−$[SCN]^-$ > $[BMIM]^+$−$[N(CN)_2]^-$ > $[BMIM]^+$−$[C(CN)_3]^-$ > $[BMIM]^+$−$[B(CN)_4]^-$, whereas CO_2 solubility increases. This is similar to the observation by Babarao et al.[16] Among the four ILs, $\Delta E_{[BMIM]^+-[B(CN)_4]^-}$ is the weakest; hence, [BMIM][B(CN)$_4$] has the loosest (least compact) structure and the highest CO_2 solubility and diffusivity. The analysis of binding energy is based on energetic effect. To more thoroughly quantify,

dx.doi.org/10.1021/jp411434g | J. Phys. Chem. C 2014, 118, 3110−3118

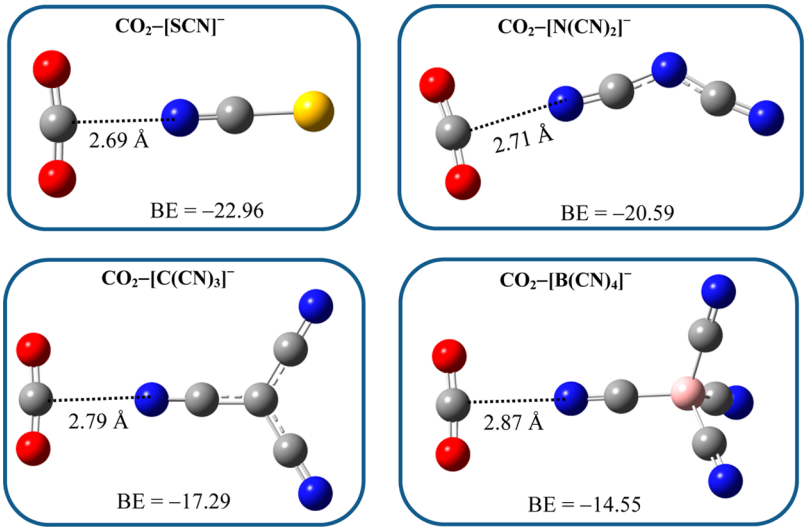

Figure 9. Optimized configurations and binding energies (kJ·mol^{-1}) of CO_2 with $[SCN]^-$, $[N(CN)_2]^-$, $[C(CN)_3]^-$, and $[B(CN)_4]^-$.

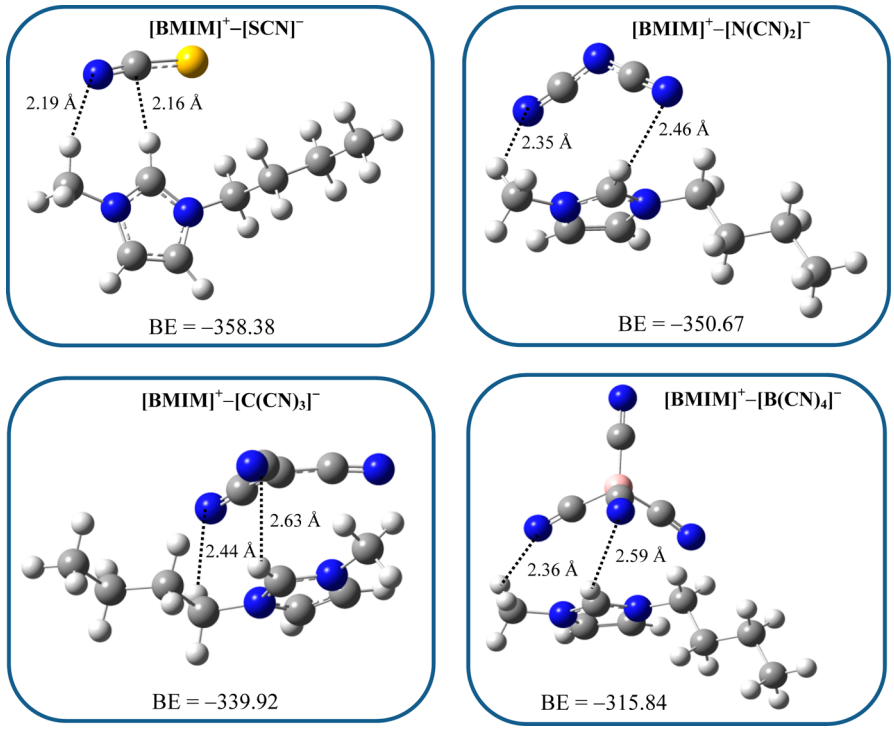

Figure 10. Optimized configurations and binding energies (kJ·mol^{-1}) of $[BMIM]^+$ with $[SCN]^-$, $[N(CN)_2]^-$, $[C(CN)_3]^-$, and $[B(CN)_4]^-$.

however, entropic effect should also be considered. Consequently, both solubility and diffusivity can be enhanced by increasing number of −CN, and $[BMIM][B(CN)_4]$ might be a promising candidate for CO_2 capture.

4. CONCLUSIONS

Nitrile (−CN) based ILs are intriguing candidates for CO_2 capture. We report a computational study to systematically examine how the number of −CN affects CO_2 sorption and diffusion. The interaction strength of cation−anion in neat ILs is found to decrease as $[BMIM][SCN] > [BMIM][N(CN)_2] > [BMIM][C(CN)_3] > [BMIM][B(CN)_4]$. This suggests that, with increasing number of −CN, the cation−anion interaction decreases; however, the cation−cation and anion−anion interactions are not significantly affected. The mobility of anion depends on not only the size/weight of anion but also the interaction with cation. For the four anions, the mobility drops in the order of $[N(CN)_2]^- > [C(CN)_3]^- > [B(CN)_4]^- > [SCN]^-$.

A minimum is observed in the potential of mean force for CO_2 moving from gas phase into IL; thus, CO_2 molecules are largely accumulated at the CO_2/IL interface. The hydrophobic butyl chain of $[BMIM]^+$ is preferentially located toward gas phase, whereas the less hydrophobic methyl group tends to reside in IL. Both solubility and diffusivity of CO_2 are found to increase with increasing number of −CN. Thus, $[BMIM][B(CN)_4]$ is the best among the four ILs for CO_2 capture. It is further revealed that CO_2 solubility is not governed by the binding energy of CO_2−anion; instead, the binding energy of cation−anion plays a more dominant role. This study, combining molecular simulation and

dx.doi.org/10.1021/jp411434g | J. Phys. Chem. C 2014, 118, 3110−3118

ab initio calculation, provides fundamental understanding for CO_2 capture in −CN based ILs, particularly, for the effect of increasing number of −CN.

■ ASSOCIATED CONTENT

Supporting Information

Atomic types and charges of $[BMIM]^+$, $[SCN]^-$, $[N(CN)_2]^-$, $[C(CN)_3]^-$, and $[B(CN)_4]^-$. Radial distribution functions for CO_2 around $[BMIM]^+$ and $[B(CN)_4]^-$ in the CO_2/[BMIM]-$[B(CN)_4]$ system. This material is available free of charge via the Internet at http://pubs.acs.org.

■ AUTHOR INFORMATION

Corresponding Author

*E-mail: chejj@nus.edu.sg.

Notes

The authors declare no competing financial interest.

■ ACKNOWLEDGMENTS

The authors are grateful to Dr. Oleg Borodin for providing the force field parameters for $[B(CN)_4]^-$, and to the National University of Singapore and the Ministry of Education of Singapore for financial support.

■ REFERENCES

(1) Quadrelli, R.; Peterson, S. The Energy-Climate Challenge: Recent Trends in CO_2 Emissions from Fuel Combustion. *Energy Policy* **2007**, *35*, 5938−5952.

(2) Stewart, C.; Hessami, M. A. A Study of Methods of Carbon Dioxide Capture and Sequestration—the Sustainability of a Photosynthetic Bioreactor Approach. *Energy Convers. Manage.* **2005**, *46*, 403−420.

(3) Le Moullec, Y.; Kanniche, M. Screening of Flowsheet Modifications for an Efficient Monoethanolamine Based Post-Combustion CO_2 Capture. *Int. J. Greenhouse Gas Control* **2011**, *5*, 727−740.

(4) Shiflett, M. B.; Drew, D. W.; Cantini, R. A.; Yokozeki, A. Carbon Dioxide Capture Using Ionic Liquid 1-Butyl-3-Methylimidazolium Acetate. *Energy Fuels* **2010**, *24*, 5781−5789.

(5) Gupta, K. M.; Hu, Z. Q.; Jiang, J. W. Mechanistic Understanding of Interactions between Cellulose and Ionic Liquids: A Molecular Simulation Study. *Polymer* **2011**, *52*, 5904−5911.

(6) Gupta, K. M.; Hu, Z. Q.; Jiang, J. W. Cellulose Regeneration from a Cellulose/Ionic Liquid Mixture: The Role of Anti-Solvents. *RSC Adv.* **2013**, *3*, 12794−12801.

(7) Zhang, X. P.; Zhang, X. C.; Dong, H. F.; Zhao, Z. J.; Zhang, S. J.; Huang, Y. Carbon Capture with Ionic Liquids: Overview and Progress. *Energy Environ. Sci.* **2012**, *5*, 6668−6681.

(8) Armand, M.; Endres, F.; MacFarlane, D. R.; Ohno, H.; Scrosati, B. Ionic-Liquid Materials for the Electrochemical Challenges of the Future. *Nat. Mater.* **2009**, *8*, 621−629.

(9) Yang, Z.; Pan, W. B. Ionic Liquids: Green Solvents for Nonaqueous Biocatalysis. *Enzyme Microb. Technol.* **2005**, *37*, 19−28.

(10) Zeng, Z.; Phillips, B. S.; Xiao, J. C.; Shreeve, J. M. Polyfluoroalkyl, Polyethylene Glycol, 1,4-Bismethylenebenzene or 1,4-Bismethylene-2,3,5,6-Tetrafluorobenzene Bridged Functionalized Dicationic Ionic Liquids: Synthesis and Properties as High Temperature Lubricants. *Chem. Mater.* **2008**, *20*, 2719−2726.

(11) Blanchard, L. A.; Hancu, D.; Beckman, E. J.; Brennecke, J. F. Green processing using ionic liquids and CO_2. *Nature* **1999**, *399*, 28−29.

(12) Aki, S. N. V. K.; Mellein, B. R.; Saurer, E. M.; Brennecke, J. F. High-Pressure Phase Behavior of Carbon Dioxide with Imidazolium-Based Ionic Liquids. *J. Phys. Chem. B* **2004**, *108*, 20355−20365.

(13) Wang, C. M.; Luo, H. M.; Jiang, D. E.; Li, H. R.; Dai, S. Carbon Dioxide Capture by Superbase-Derived Protic Ionic Liquids. *Angew. Chem., Int. Ed.* **2010**, *49*, 5978−5981.

(14) Wang, C. M.; Luo, X. Y.; Luo, H. M.; Jiang, D. E.; Li, H. R.; Dai, S. Tuning the Basicity of Ionic Liquids for Equimolar CO_2 Capture. *Angew. Chem., Int. Ed.* **2011**, *50*, 4918−4922.

(15) Cadena, C.; Anthony, J. L.; Shah, J. K.; Morrow, T. I.; Brennecke, J. F.; Maginn, E. J. Why Is CO_2 So Soluble in Imidazolium-Based Ionic Liquids? *J. Am. Chem. Soc.* **2004**, *126*, 5300−5308.

(16) Babarao, R.; Dai, S.; Jiang, D. E. Understanding the High Solubility of CO_2 in an Ionic Liquid with the Tetracyanoborate Anion. *J. Phys. Chem. B* **2011**, *115*, 9789−9794.

(17) Perez-Blanco, M. E.; Maginn, E. J. Molecular Dynamics Simulations of CO_2 at an Ionic Liquid Interface: Adsorption, Ordering, and Interfacial Crossing. *J. Phys. Chem. B* **2012**, *116*, 9285−9285.

(18) Carlisle, T. K.; Bara, J. E.; Gabriel, C. J.; Noble, R. D.; Gin, D. L. Interpretation of CO_2 Solubility and Selectivity in Nitrile-Functionalized Room-Temperature Ionic Liquids Using a Group Contribution Approach. *Ind. Eng. Chem. Res.* **2008**, *47*, 7005−7012.

(19) Gonzalez-Miquel, M.; Palomar, J.; Omar, S.; Rodriguez, F. CO_2/N_2 Selectivity Prediction in Supported Ionic Liquid Membranes by COSMO-RS. *Ind. Eng. Chem. Res.* **2011**, *50*, 5739−5748.

(20) Mahurin, S. M.; Lee, J. S.; Baker, G. A.; Luo, H. M.; Dai, S. Performance of Nitrile-Containing Anions in Task-Specific Ionic Liquids for Improved CO_2/N_2 Separation. *J. Membr. Sci.* **2010**, *353*, 177−183.

(21) Mahurin, S. M.; Hillesheim, P. C.; Yeary, J. S.; Jiang, D. E.; Dai, S. High CO_2 Solubility, Permeability and Selectivity in Ionic Liquids with the Tetracyanoborate Anion. *RSC Adv.* **2012**, *2*, 11813−11819.

(22) Gupta, K. M.; Chen, Y.; Hu, Z.; Jiang, J. Metal−Organic Framework Supported Ionic Liquid Membranes for CO_2 Capture: Anion Effects. *Phys. Chem. Chem. Phys.* **2012**, *14*, 5785−5794.

(23) Cornell, W. D.; Cieplak, P.; Bayly, C. I.; Gould, I. R.; Merz, K. M.; Ferguson, D. M.; Spellmeyer, D. C.; Fox, T.; Caldwell, J. W.; Kollman, P. A. A Second Generation Force Field for the Simulation of Proteins, Nucleic Acids, and Organic Molecules. *J. Am. Chem. Soc.* **1995**, *117*, 5179−5197.

(24) Borodin, O. Polarizable Force Field Development and Molecular Dynamics Simulations of Ionic Liquids. *J. Phys. Chem. B* **2009**, *113*, 11463−11478.

(25) Mayo, S. L.; Olafson, B. D.; Goddard, W. A. Dreiding—A Generic Force-Field for Molecular Simulations. *J. Phys. Chem.* **1990**, *94*, 8897−8909.

(26) Frisch, M. J.; Trucks, G. W.; Schlegel, H. B.; Scuseria, G. E.; Robb, M. A.; Cheeseman, J. R.; Zakrzewski, V. G.; Montgomery, J. A.; Stratmann, R. E.; Burant, J. C.; Dapprich, S.; Millam, J. M.; Daniels, A. D.; Kudin, K. N.; Strain, M. C.; Farkas, O.; Tomasi, J.; Barone, V.; Cossi, M.; Cammi, R.; Mennucci, B.; Pomelli, C.; Adamo, C.; Clifford, S.; Ochterski, J.; Petersson, G. A.; Ayala, P. Y.; Cui, Q.; Morokuma, K.; Malick, D. K.; Rabuck, A. D.; Raghavachari, K.; Foresman, J. B.; Cioslowski, J.; Ortiz, J. V.; Stefanov, B. B.; Liu, G.; Liashenko, A.; Piskorz, P.; Komaromi, I.; Gomperts, R.; Martin, R. L.; Fox, D. J.; Keith, T.; Al-Laham, M. A.; Peng, C. Y.; Nanayakkara, A.; Gonzalez, C.; Challacombe, M.; Gill, P. M. W.; Johnson, B. G.; Chen, W.; Wong, M. W.; Andres, J. L.; Head-Gordon, M.; Replogle, E. S.; Pople, J. A. *Gaussian 09*, Revision D.01; Gaussian, Inc.: Wallingford, CT, 2009.

(27) Singh, U. C.; Kollman, P. A. An Approach to Computing Electrostatic Charges for Molecules. *J. Comput. Chem.* **1984**, *5*, 129−145.

(28) van Der Spoel, D.; Lindahl, E.; Hess, B.; Groenhof, G.; Mark, A. E.; Berendsen, H. J. C. Gromacs: Fast, Flexible, and Free. *J. Comput. Chem.* **2005**, *26*, 1701−1718.

(29) Berendsen, H. J. C.; Postma, J. P. M.; Vangunsteren, W. F.; Dinola, A.; Haak, J. R. Molecular-Dynamics with Coupling to an External Bath. *J. Chem. Phys.* **1984**, *81*, 3684−3690.

(30) Torrie, G. M.; Valleau, J. P. Non-Physical Sampling Distributions in Monte Carlo Free-Energy Estimation—Umbrella Sampling. *J. Comput. Phys.* **1977**, *23*, 187−199.

(31) Kumar, S.; Bouzida, D.; Swendsen, R. H.; Kollman, P. A.; Rosenberg, J. M. The Weighted Histogram Analysis Method for Free-Energy Calculations on Biomolecules. The Method. *J. Comput. Chem.* **1992**, *13*, 1011−1021.

(32) Moller, C.; Plesset, M. S. Note on an Approximation Treatment for Many-Electron Systems. *Phys. Rev.* **1934**, *46*, 618−622.
(33) Boys, S. F.; Bernardi, F. The Calculations of Small Molecular Interaction by the Difference of Separate Total Energies—Some Procedures with Reduced Error. *Mol. Phys.* **1970**, *19*, 553−566.
(34) Domanska, U.; Krolikowska, M. Density and Viscosity of Binary Mixtures of {1-Butyl-3-Methylimidazolium Thiocyanate + 1-Heptanol, 1-Octanol, 1-Nonanol, or 1-Decanol}. *J. Chem. Eng. Data* **2010**, *55*, 2994−3004.
(35) Gupta, K. M.; Hu, Z. Q.; Jiang, J. W. Molecular Insight into Cellulose Regeneration from a Cellulose/Ionic Liquid Mixture: Effects of Water Concentration and Temperature. *RSC Adv.* **2013**, *3*, 4425−4433.
(36) Tsuzuki, S.; Shinoda, W.; Saito, H.; Mikami, M.; Tokuda, H.; Watanabe, M. Molecular Dynamics Simulations of Ionic Liquids: Cation and Anion Dependence of Self-Diffusion Coefficients of Ions. *J. Phys. Chem. B* **2009**, *113*, 10641−10649.
(37) Del Popolo, M. G.; Voth, G. A. On the Structure and Dynamics of Ionic Liquids. *J. Phys. Chem. B* **2004**, *108*, 1744−1752.
(38) Maginn, E. J. Atomistic Simulation of the Thermodynamic and Transport Properties of Ionic Liquids. *Acc. Chem. Res.* **2007**, *40*, 1200−1207.
(39) Roscioli, J. R.; Nesbitt, D. J. State-Resolved Scattering at Room-Temperature Ionic Liquid−Vacuum Interfaces: Anion Dependence and the Role of Dynamic Versus Equilibrium Effects. *J. Phys. Chem. Lett.* **2010**, *1*, 674−678.
(40) Perez-Blanco, M. E.; Maginn, E. J. Molecular Dynamics Simulations of Carbon Dioxide and Water at an Ionic Liquid Interface. *J. Phys. Chem. B* **2011**, *115*, 10488−10499.
(41) Bhargava, B. L.; Krishna, A. C.; Balasubramanian, S. Molecular Dynamics Simulation Studies of CO_2 - [Bmim][PF_6] Solutions: Effect of CO_2 Concentration. *AIChE J.* **2008**, *54*, 2971−2978.
(42) Wick, C. D.; Chang, T. M.; Dang, L. X. Molecular Mechanism of CO_2 and SO_2 Molecules Binding to the Air/Liquid Interface of 1-Butyl-3-Methylimidazolium Tetrafluoroborate Ionic Liquid: A Molecular Dynamics Study with Polarizable Potential Models. *J. Phys. Chem. B* **2010**, *114*, 14965−14971.
(43) Dang, L. X.; Chang, T. M. Molecular Mechanism of Gas Adsorption into Ionic Liquids: A Molecular Dynamics Study. *J. Phys. Chem. Lett.* **2012**, *3*, 175−181.
(44) Sudha, S. Y.; Khanna, A. Evaluating the Interactions of CO_2-Ionic Liquid Systems through Molecular Modeling. *World Acad. Sci., Eng. Technol.* **2009**, *57*, 539−542.
(45) Bhargava, B. L.; Balasubramanian, S. Probing Anion-Carbon Dioxide Interactions in Room Temperature Ionic Liquids: Gas Phase Cluster Calculations. *Chem. Phys. Lett.* **2007**, *444*, 242−246.
(46) Kazarian, S. G.; Briscoe, B. J.; Welton, T. Combining Ionic Liquids and Supercritical Fluids: In Situ ATR-IR Study of CO_2 Dissolved in Two Ionic Liquids at High Pressures. *Chem. Commun.* **2000**, 2047−2048.

Supporting Information

Systematic Investigation of Nitrile-Based Ionic Liquids for CO_2 Capture: A Combination of Molecular Simulation and *Ab Initio* Calculation

Krishna M. Gupta and Jianwen Jiang*

Department of Chemical and Biomolecular Engineering, National University of Singapore, 117576, Singapore

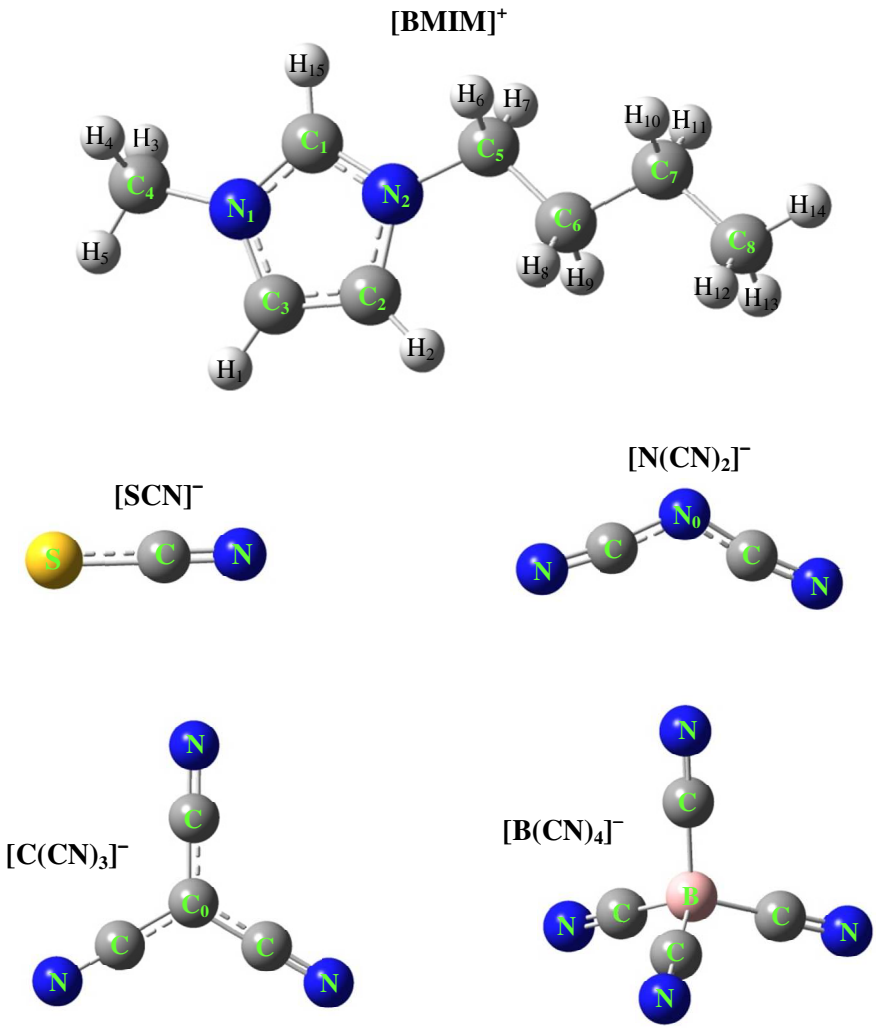

Figure S1. Atomic types of $[BMIM]^+$, $[SCN]^-$, $[N(CN)_2]^-$, $[C(CN)_3]^-$, and $[B(CN)_4]^-$.

Table S1. Atomic charges of $[BMIM]^+$, $[SCN]^-$, $[N(CN)_2]^-$, $[C(CN)_3]^-$, and $[B(CN)_4]^-$.

$[BMIM]^+$

Atom	C_1	C_2	C_3	C_4	C_5	C_6	C_7	C_8	N_1	N_2
Charge	-0.158	-0.151	-0.236	-0.316	-0.342	0.136	0.112	-0.315	0.218	0.276
Atom	H_1	H_2	H_3	H_4	H_5	H_6	H_7	H_8	H_9	H_{10}
Charge	0.205	0.251	0.162	0.164	0.170	0.143	0.145	0.009	0.009	0.009
Atom	H_{11}	H_{12}	H_{13}	H_{14}	H_{15}					
Charge	0.008	0.082	0.111	0.079	0.230					

$[SCN]^-$

Atom	S	C	N
Charge	-0.722	0.459	-0.737

$[N(CN)_2]^-$

Atom	N_0	C	N
Charge	-0.698	0.620	-0.771

$[C(CN)_3]^-$

Atom	C_0	C	N
Charge	-1.000	0.692	-0.692

$[B(CN)_4]^-$

Atom	B	C	N
Charge	-0.316	0.376	-0.547

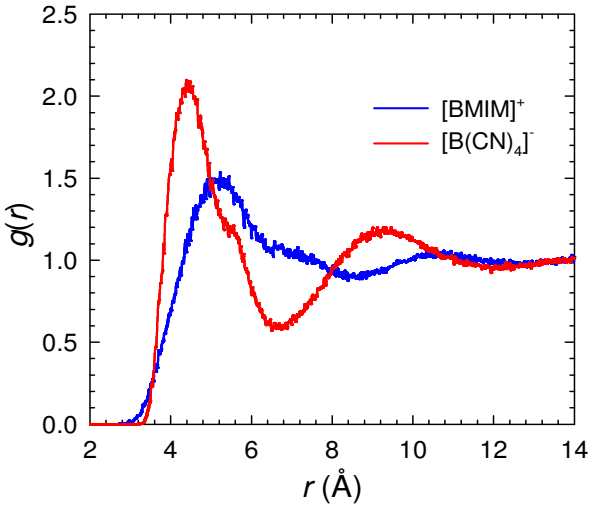

Figure S2. Radial distribution functions for CO_2 around $[BMIM]^+$ and $[B(CN)_4]^-$ in CO_2/[BMIM][$B(CN)_4$] system.